Dynamic Buckling of Continuous Welded Rail Track: Theory, Tests, and Safety Concepts

A. KISH AND G. SAMAVEDAM

A versatile, dynamic buckling model that can be used on a personal computer is presented. The model accounts for vehicle load influences and nonlinearities in track resistance, hitherto ignored in the literature. These influences are shown to be important in the accurate predictions of buckling response and hence in buckling safety considerations. The model also computes the energy required to buckle the track and thus indicates the levels of safety at given rail temperatures. On the basis of the energy and the upper and lower buckling temperatures derived from the model, rational buckling safety criteria have been developed. Results of controlled full-scale dynamic buckling tests conducted on tangent, 5-, and 7.5-degree continuous welded rail track are presented and correlated with theoretical predictions from the model on buckling temperatures, forces, and safety limits.

Thermal buckling of continuous welded rail (CWR) track is an important problem facing the safe operation of railroads in the United States. Increased utilization of CWR and recent trends toward higher speeds and heavier axle loads are expected to exacerbate this problem. In an effort to improve the safety of CWR track, analytical and experimental investigations have been conducted by the Transportation Systems Center (TSC) in support of the safety mission of FRA. Investigations of CWR track buckling under thermally induced forces and vehicle loads are described in this paper.

The TSC approach to the solution of the buckling problem consists of

- Developing a rigorous model based on fundamental principles of structural mechanics that accounts for all significant parameters,
- Validating the model by controlled full-scale field tests, and
- Developing rational safety criteria for use by the industry.

Static buckling is defined as the buckling of long CWR tracks caused by thermal load alone with no interaction from vehicles. Most of the published literature deals with this type of buckling. In contrast, dynamic buckling, which is more relevant to the industry, is defined as the instability of CWR track under moving vehicles in the presence of thermal loads. The dynamic buckling aspects of CWR track are the focus of this paper.

A. Kish, Transportation Systems Center, DTS-76, 55 Broadway, Cambridge, Mass. 02142. G. Samavedam, Foster-Miller, Inc., 350 Second Avenue, Waltham, Mass. 02254.

REVIEW OF STATIC BUCKLING

Before the development of dynamic buckling theory, TSC conducted theoretical studies and field tests of static buckling. The studies were based on early work by Kerr (*1*) and Samavedam (*2*). Kerr's work defined the basic large deflection analysis required in the thermal buckling problem for tangent tracks. Samavedam generalized the various nonlinearities in the input parameters and proposed the first rigorous analysis for curved tracks.

In 1982 Kish et al. (*3*) conducted the first series of static buckling tests on U.S. mainline tangent and 5-degree-curve track to better define the buckling response mechanism and characteristics. A significant number of theoretical parametric studies on static buckling have also been conducted (*4*). These and subsequent research efforts have clearly identified the need for a more comprehensive analytic model that incorporates several nonlinear parameters and dynamic effects and for rational buckling safety criteria.

Recent advances in the analytic modeling of the dynamic buckling behavior of CWR track, some relevant validation tests, and proposed safety criteria that may provide a basis for rational guidelines for buckling prevention are presented here.

LIMITATIONS OF EXISTING THEORIES

Before 1985, all known theories published in the United States and elsewhere had three major deficiencies:

- Inadequate representation of lateral resistance,
- Lack of vehicle load effects, and
- No rational criteria for CWR buckling safety.

In 1985, Kish et al. (*5*) published the first work on dynamic buckling, which covered various buckling mechanisms arising from vehicle loads. This work recently has been extended to rectify the deficiencies listed above.

For further development, appropriate terminology must be introduced. The lateral buckling response can be expressed in the form of a relationship between the maximum lateral track displacement and the temperature increase over the force-free or neutral temperature, as shown in Figure 1.

At point B, the structure becomes unstable, even under an infinitesimal disturbance. $T_{B,\max}$ is the upper buckling temperature, the maximum temperature limit before the track buckles. The track could also buckle at $T_{B,\min}$ from its stable

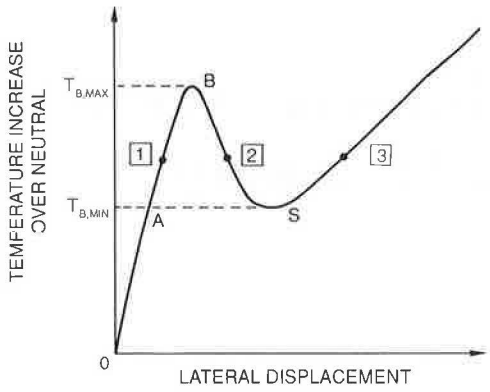

FIGURE 1 Typical buckling response.

equilibrium position A to S, if given sufficient external disturbance, such as forces developed by a moving train. $T_{B,\min}$ is defined as the lower buckling temperature, which, as seen later, may or may not equal a safe allowable temperature.

Lateral Resistance Characteristic

TSC performed a large number of track lateral resistance evaluation tests. Both panel pull and single-tie push tests (STPTs) were executed and the results were correlated. As described by the authors in another paper in this Record, a special portable test fixture for individual tie resistance evaluation has been developed. Typical results for U.S. track are shown in Figure 2. The results identify two salient points, F_p and F_L, which are the peak resistance and the limiting resistance. Except in the case of extremely weak tracks, the resistance has a "softening" characteristic after reaching the peak value. The full characteristic is important in the buckling analysis because at temperatures equal to or greater than the lower buckling temperature ($T_{B,\min}$) the resulting deflections are large. Many existing works considered only the peak resistance in the determination of the buckling response and significantly overestimated the values of $T_{B,\min}$, the implications of which will be discussed later.

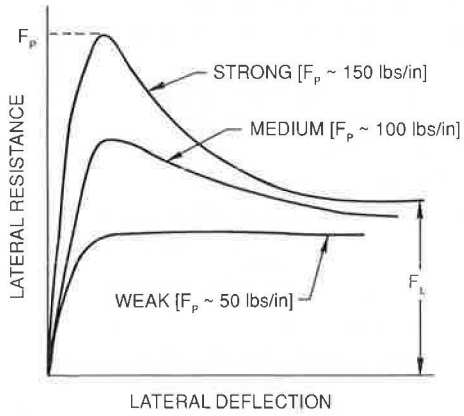

FIGURE 2 Typical single-tie push test results.

Vehicle Load Effects

Research conducted by the French National Railway (SNCF) indicates that most track buckling is caused by vehicle passage (*6*). According to a survey by the Association of American Railroads, 68 percent of derailment-inducing buckling occurred under the train consist; 6 percent occurred in front of the locomotive (*7*). Tests conducted by the Hungarian State Railways indicated that vehicle traffic can reduce the buckling strength by 20 to 30 percent (*8,9*). These data and the results of testing by TSC, which will be presented later, indicate the importance of including vehicle effects in buckling analyses.

Work by Kish et al. (*5*) contains a review of literature on vehicle effects published before 1985. The following mechanisms were identified to be important in constructing an appropriate dynamic buckling theory:

1. Uplift of the track due to precession/recession and central bending waves can reduce the lateral resistance and, hence, buckling strength.
2. Lateral forces generated on the track due to wheel/rail interaction (especially in the presence of lateral imperfections), in combination with many passes of the vehicle, can increase the size of the imperfection and therefore reduce the buckling strength.
3. Braking, traction, and flanging forces can also increase compressive forces and hence reduce buckling strength.
4. Track vibration caused by passage of a vehicle can cause loss of lateral ballast resistance.

Detailed calculations on Mechanism 1 are presented in work by Kish et al. (*5*). The central bending wave for long cars and the precession wave for locomotives are generally important in buckling evaluation, as shown in Figure 3. The work presented in this paper accounts for the loss of lateral resistance caused by the uplift of the track, allowing for self-weight of the track. The uplift mechanism has been previously identified as one of the principal causes of buckling by European researchers, including Eisenmann (*10*). An experimental proof of the effect of this mechanism will be provided later.

The effect of the ratio of truck lateral to vertical loads (L/V), as implied in Mechanism 2, was considered by Kish et al., who concluded that L/V becomes critical if it exceeds the friction coefficient between tie and ballast (*5*). The same conclusion was reached earlier by SNCF (*6*). Limited studies have been performed to date on Mechanism 3, and no work has been done in the United States on Mechanism 4. The TSC approach is to combine the influence of those dynamic factors into a dynamic margin of safety, which will be discussed later.

Basis for Buckling Safety Criteria

Previous works recommend the lower buckling temperature as the safe allowable limit for CWR track. As shown later, this approach can be conservative in some cases. An optimum safe allowable temperature must therefore be established. This can be done through energy considerations presented here.

At the upper buckling temperature, the external energy required to buckle the track is zero. This temperature cannot practically be reached without buckling the track under dy-

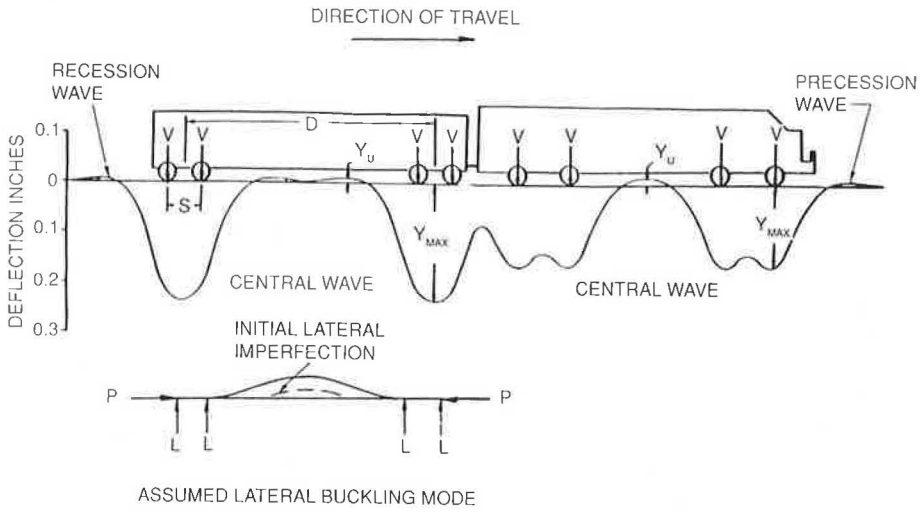

FIGURE 3 Typical track deflections caused by GP38-2 locomotive and hopper car.

namic conditions because trains always cause some finite disturbance. Nevertheless, the energy required to buckle the track at the lower buckling temperature may be considerably greater than that generated by moving trains. The track's buckling potential at different rail temperatures for given parameters can be evaluated through calculation of the energy required for buckling. As shown later, energy calculations provide a rational basis for defining operational temperatures with a given level of safety.

TSC BUCKLING MODEL

A buckling model has been developed by TSC using the differential equations described in the next section. It has the following features:

- It applies to tangent and curved tracks.
- Lateral alignment defects are included.
- It accounts for any nonlinearity in the lateral resistance, including the softening behavior referred to previously. The individual contributions of tie bottom, crib, and shoulder to the lateral resistance become important in the model.
- Linear or nonlinear longitudinal resistance can be incorporated.
- It considers vehicle load influences and accounts for lateral resistance loss or variation under the cars. Car parameters such as truck center spacing and wheel load are included, as are track modulus and tie-ballast friction coefficient.
- It calculates the external energy required for an explosive (sudden) buckling and thus indicates the potential risk of buckling at a given rise in rail temperature.
- It can be run on a personal computer (PC), with simple user-friendly inputs. It can be operated as an expert system, requiring no knowledge of the theoretical equations involved. The program has default options and automatically assumes missing input if not provided by the operator.
- The output can be in the form of buckling response curves, with printout of upper and lower buckling temperatures, energy, and risk factors.
- Within the limitations of the physical assumptions, the model is extremely accurate, relying on differential equations and fast converging Fourier series solution.

Buckling Response Determination

A basic formulation for tangent track has been provided by Samavedam et al. (*11*). Here, the formulation for curved track not presented in earlier work is given. The following assumptions are made:

- The two rails can be combined into a single beam of known cross-sectional area A and flexural rigidity EI.
- The torsional stiffness in rail-tie fasteners may be neglected, which is reasonable for the majority of wood-tie tracks with tie plate–cut spike construction in the United States.
- The buckled zone with lateral displacements is confined to a finite length. This has been confirmed by tests (*12,13*). The longitudinal resistance offered by the ballast to the longitudinal movement of the rail beam can be neglected in the buckled zone, which will simplify the solution of the resulting differential equations.
- The adjoining zone experiences only longitudinal movement, and the rail force at infinity is $P_\infty = AE\alpha T$, where T is the increase in temperature over the stress-free temperature and α is the rail steel's coefficient of thermal expansion. The longitudinal resistance can be linear or nonlinear. As shown by Samavedam (*2*), there are no theoretical difficulties in handling the nonlinearity in the resistance. For simplicity, linear idealization will be used here because it appears to be adequate, on the basis of recent field test data.

The lateral resistance is idealized as follows.

Partial "softening" lateral resistance:

$$F[w(x)] = F_p[k + (1 - k)\exp(-\mu_2 w)] \tag{1.1}$$

Full "softening" lateral resistance:

$$F[w(x)] = F_p[1 - \exp(-\mu_1 w)]\left\{k + (1 - k) \times \exp\left[-\mu_2\left(w - \frac{4}{\mu_1}\right)\right]\right\} \quad (1.2)$$

where

F_p = value of the peak lateral resistance,
k = ratio of reduced to peak lateral resistance,
μ_1 and μ_2 = stiffness parameters that define the initial and softening behavior of the assumed lateral resistance function, and
w = lateral or radial track deflection.

Examples of the idealizations are shown in Figure 4.

For the case in which vehicle loading is present, the peak resistance (F_p) is a function of the longitudinal distance along the track:

$$\overline{F}_p[w(x)] = \begin{cases}[F_p - \mu Q] \text{ for uplift} \\ [F_p + \mu R_v(x)] \text{ otherwise}\end{cases} \quad (2)$$

where

F_p = peak value of static lateral resistance,
μ = tie to ballast coefficient of friction,
Q = self-weight of the entire track, and
$R_v(x)$ = vertical deflection profile produced by the vehicle wheel loads on the track.

The vertical deflection profile can be calculated from the classical theory for beams on elastic foundation. Uplift occurs when the sum of the vertical deflection and the self-weight of the track is less than zero ($[Q + R_v(x)] < 0$).

Governing Equations for Curved Track Analysis

For the geometry and coordinate system shown in Figure 5, the governing differential equation in the buckled zone ($0 \leq \Theta \leq \phi$) for curved track is given by Samavedam (2) as

$$\frac{EI_{zz}}{R^4}\frac{d^4w}{d\Theta^4} + \frac{\overline{P}}{R^2}\frac{d^2w}{d\Theta^2} = -F[w(\Theta)] + \frac{\overline{P}}{R} - \frac{\overline{P}}{R^2}\frac{d^2w_o}{d\Theta^2} \quad (3)$$

where

EI_{zz} = flexural rigidity of both rails in the lateral plane,
$\overline{P}$ = rail compressive force,
w = lateral or radial displacement,
w_o = initial misalignment, and
F = the lateral resistance.

The Fourier method originally given by Samavedam (2) is used for the solution of Equation 3:

$$w(\Theta) = \sum_{m=1,3,5\ldots}^{\infty} A_m \cos\left(\frac{m\pi\Theta}{2\phi}\right) \quad (4.1)$$

$$\frac{\overline{P}}{R^2}\frac{d^2w_o}{dx^2} = \sum_{m=1,3,5\ldots}^{\infty} b_m \cos\left(\frac{m\pi\Theta}{2\phi}\right) \quad (4.2)$$

$$F[w(x)] = \sum_{m=1,3,5\ldots}^{\infty} a_m \cos\left(\frac{m\pi\Theta}{2\phi}\right) \quad (4.3)$$

$$\frac{\overline{P}}{R} = \sum_{m=1,3,5\ldots}^{\infty} c_m \cos\left(\frac{m\pi\Theta}{2\phi}\right) \quad (4.4)$$

Using the differential equation, it can be shown that

$$A_m = \frac{-\left[\left(a_m - \frac{\overline{P}}{R}c_m\right) + \frac{\overline{P}}{R^2}b_m\right]}{\left[\frac{EI_{zz}}{R^4}\left(\frac{m\pi}{2\phi}\right)^4 - \frac{\overline{P}}{R^2}\left(\frac{m\pi}{2\phi}\right)^2\right]} \quad (5)$$

The Fourier coefficient that accounts for the effects of lateral resistance in the curved track case is derived from

$$a_m = \frac{2}{\phi}\int_0^{\phi} F[w(\Theta)] \cos\left(\frac{m\pi\Theta}{2\phi}\right) d\Theta \quad (6.1)$$

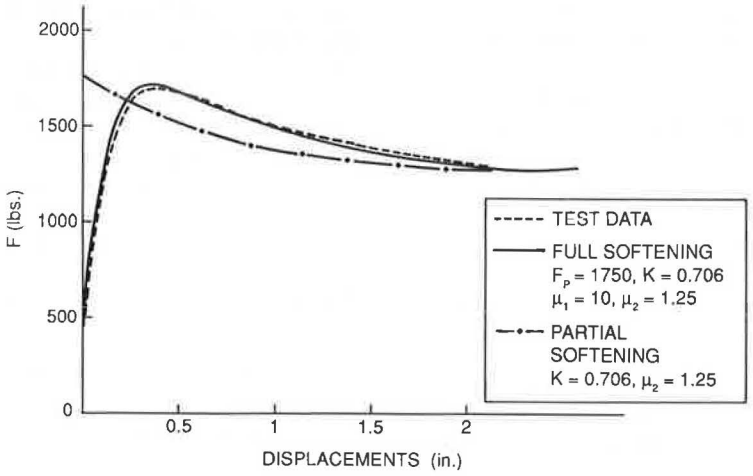

FIGURE 4 Lateral resistance test data and idealizations.

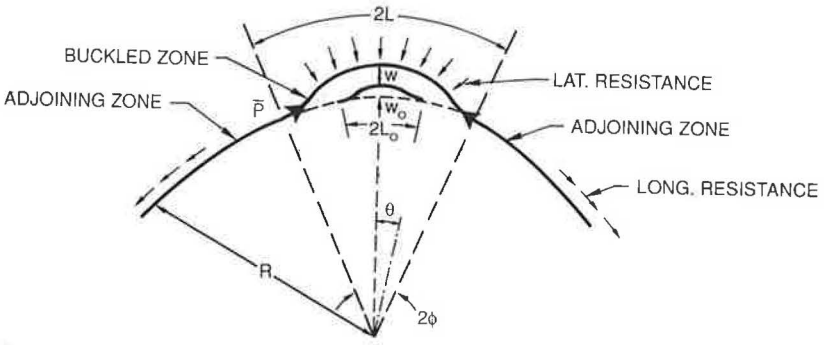

FIGURE 5 Geometry and coordinates for curved track.

This integral is evaluated numerically by using Filon's method.

The Fourier coefficient that accounts for the effect of imperfection is obtained from the following integral:

$$b_m = \frac{2}{\phi}\int_0^{\phi^*} \frac{d^2 w_o}{d\Theta^2} \cos\left(\frac{m\pi\Theta}{2\phi}\right) d\Theta \tag{6.2}$$

where

$$\phi^* = \begin{cases} \phi & \text{if } \phi \le \phi_o \\ \phi_o & \text{if } \phi > \phi_o \end{cases}$$

A quartic imperfection shape is assumed (although the analysis is capable of dealing with any form of imperfection) as

$$w(\Theta) = \delta_o\left[1 - 2\left(\frac{\Theta}{\phi_o}\right)^2 + \left(\frac{\Theta}{\phi_o}\right)^4\right] \tag{7.1}$$

where δ_o is the "offset" or the amplitude and $2R\phi_o = 2L_o$ is the length over which the imperfection occurs. Thus, evaluation of the integral for b_m results in the following:

If $\phi \le \phi_o$,

$$\frac{b_m}{R^2} = -\frac{16\,\delta_o}{m\pi L_o^2}\left\{1 - 3\left(\frac{L}{L_o}\right)^2 \times \left[1 - 2\left(\frac{2}{m\pi}\right)^2\right]\right\} \sin\left(\frac{m\pi}{2}\right) \tag{7.2}$$

If $\phi > \phi_o$,

$$\frac{b_m}{R^2} = -\frac{16\,\delta_o}{m\pi L_o^2}\left\{-6\left(\frac{L}{L_o}\right)\left(\frac{2}{m\pi}\right)\cos\left(\frac{m\pi L_o}{2L}\right) + 2\left[-1 + 3\left(\frac{2L}{m\pi L_o}\right)^2\right]\sin\left(\frac{m\pi L_o}{2L}\right)\right] \tag{7.3}$$

Note that $\phi = L/R$ and $\phi_o = L_o/R$.

The remaining Fourier coefficient is

$$c_m = \frac{2}{\phi}\int_0^{\Phi} \cos\left(\frac{m\pi\Theta}{2\phi}\right) d\Theta = \frac{4}{m\pi}\sin\left(\frac{m\pi}{2}\right) \tag{7.4}$$

The differential equation of longitudinal equilibrium that applies to the adjoining region ($\Theta > \phi$) and assuming proportional longitudinal resistance is

$$\frac{AE}{R^2}\frac{d^2U}{d\Theta^2} = K_f U \tag{8.1}$$

where U is the longitudinal or tangential displacement and K_f is the longitudinal stiffness. The general solution to this equation is

$$U(\Theta) = C_3 e^{+R\Psi\Theta} + C_4 e^{-R\Psi\Theta} \tag{8.2}$$

where $\Psi^2 = K_f/AE$. The temperature equation for curved track analysis is derived from the following boundary conditions:

$$\frac{U(\phi)}{R} = -\frac{\bar{P}\phi}{AE} - Z + \alpha T\phi \tag{8.3}$$

$$\frac{U'(\phi)}{R} = -\frac{\bar{P}}{AE} + \alpha T \tag{8.4}$$

The appropriate boundary conditions must be substituted into the solution, and it must be noted that $L = R\phi$. Solving for temperature results in the following expression:

$$T = \frac{\bar{P}}{AE\alpha} + \frac{ZR\Psi}{\alpha(1 + \Psi L)} \tag{9.1}$$

where

$$ZR = \int_0^{\phi}\left(\frac{w}{R} + \frac{w'^2}{2R^2} + \frac{w'w_o'}{R^2}\right) Rd\Theta \tag{9.2}$$

$$ZR = \sum_{m=1,3,5,\ldots}^{\infty}\left[\frac{2L}{m\pi R^2} A_m \sin\left(\frac{m\pi}{2}\right) + \left(\frac{m\pi}{2}\right)^2 \frac{A_m^2}{4L} - \frac{A_m B_{mL}}{2R^2}\right] \tag{10}$$

Energy Required for Buckling

The prebuckling state is represented by Position 1 in Figure 1, and the postbuckling unstable branch is represented by Position 2. It is assumed that if the track can be brought into Position 2, it will automatically move to Position 3.

The following factors are defined:

V_1 = strain energy in the rails at stable equilibrium Position 1,
V_2 = strain energy in the rails at unstable equilibrium Position 2,
W = work done against resistances by moving track from Position 1 to Position 2, and
Ω = energy required to move track from Position 1 to Position 2.

By an energy balance

$$\Omega = (V_2 - V_1) + W \tag{11}$$

The strain energy components are given by the following integrals:

$$V_1 = \frac{1}{2}\int_0^{\infty} \frac{P_\infty^2}{AE}\,dx \tag{12}$$

where $P_\infty = -AE\alpha T$. Here, for simplicity, the energy caused by bending in the prebuckling state is neglected:

$$V_2 = \frac{1}{2}\int_0^{\infty} \frac{P^2}{AE}\,dx + \frac{EI_{zz}}{2}\int_0^{\infty}\left(\frac{d^2w}{dx^2}\right)^2 dx \tag{13}$$

In the curved track case, the longitudinal force distribution becomes

$$P = \begin{cases} \overline{P} & \text{for } 0 \le \Theta \le \phi \\ AE\left(\dfrac{1}{R}\dfrac{du}{d\Theta} - \alpha T\right) & \text{for } \Theta > \phi \end{cases} \tag{14}$$

The work components are given by the following integrals:

$$W_1 = \int_0^{\infty}\int_0^{w(x)} F[w(x)]dw{\cdot}dx \tag{15}$$

$$W_2 = \int_0^{\infty}\int_0^{u(x)} f[u(x)]du{\cdot}dx \tag{16}$$

Thus, the total work done against ballast resistance (lateral and longitudinal) is

$$W = W_1 + W_2 \tag{17}$$

The difference in strain energy is calculated from the following equation:

$$V_2 - V_1 = \frac{1}{2}\int_0^{\infty}\frac{P^2 - P_\infty^2}{AE}\,dx + \frac{EI_{zz}}{2}\int_0^{\infty}\left(\frac{d^2w}{dx^2}\right)^2 dx \tag{18}$$

This equation shows that the total strain energy is the sum of two components: one caused by compressive axial force and the other caused by beam bending. The evaluation of these integrals is performed with the aid of the Fourier analysis. Under the assumption of proportional longitudinal resistance, the difference in strain energy can be expressed in a "closed form":

$$V_2 - V_1 = \frac{AE}{2}\left\{\frac{\overline{P}}{AE}\left[\frac{\overline{P}}{AE}\left(L + \frac{1}{2\Psi}\right) + \frac{\alpha T}{\Psi}\right] - (\alpha T)^2\left(L + \frac{3}{2\Psi}\right)\right\} + \frac{EI_{zz}}{64\,L^3}\sum_{m=1,3,5,\ldots}^{\infty}(m\pi)^4 A_m^2 \tag{19}$$

The work done against lateral resistance can be evaluated from Equation 15 once the lateral resistance function is expressed mathematically. For the partial softening lateral resistance characteristics considered in the Fourier analysis section, the work done against lateral resistance is

$$W_1 = 2\int_0^{L}\overline{F}_p(x)\left[kw(x) + \left\{\frac{(1-k)}{\mu_2}1 - \exp[-\mu_2 w(x)]\right\}\right]dx \tag{20.1}$$

Full softening lateral resistance is

$$W_1 = 2\int_0^{L}\overline{F}_p(x)\left(kw(x) + \frac{k}{\mu_2}\{1 - \exp[-\mu\, w_1(x)]\}\,dx + \frac{(1-k)}{\mu_2}\exp\frac{4\mu_2}{\mu_1}\{1 - \exp[-\mu_2 w(x)]\} - \frac{(1-k)}{\mu_1+\mu_2}\exp\frac{4\mu_2}{\mu_1}\{1 - \exp[-(\mu_1+\mu_2)w(x)\}\right)dx \tag{20.2}$$

This integral is evaluated numerically.

The work done against longitudinal resistance,

$$W_2 = \frac{K_f}{4\,\Psi^3}\left(\frac{\overline{P}}{AE} - \alpha T\right)^2 \tag{21}$$

Illustrative Numerical Examples

Effect of Softening Lateral Resistance

The dynamic buckling response of 7.5-degree CWR curved track with both constant and softening lateral resistance characteristics is shown in Figure 6. The constant resistance idealization significantly overestimates the lower buckling temperature (77°F) compared with the softening characteristic (50°F). The buckling responses are also significantly different.

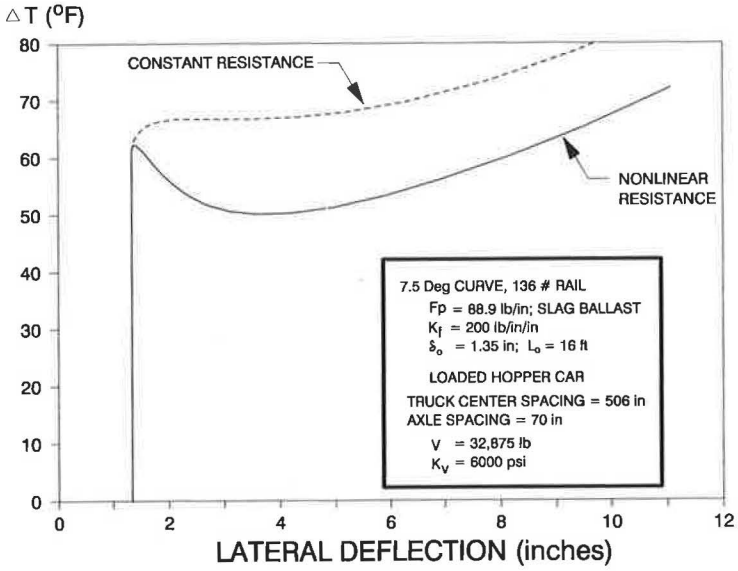

FIGURE 6 Influence of constant versus nonlinear resistance on buckling response.

Effect of Vehicle Loads

The theoretical buckling response of the 7.5-degree CWR curved track under hopper car loads is shown in Figure 7. The results for the static case without the vehicle are also shown. Because of the vehicle influence, the upper buckling temperature is reduced from 75° to 62°F.

Energy Required for Buckling

Figures 8 and 9 show the theoretical external energy required to buckle the tangent and 5-degree curved track with assumed parameters. This energy is clearly zero at the upper buckling temperature; hence, the track will buckle at this temperature. Buckling at the lower temperature requires a finite amount of energy. The energy required to buckle the track drops significantly with increased curvature and with line defects. The figures also indicate a rapid decrease in energy required with an increase in rail temperature above the lower buckling temperature.

BUCKLING SAFETY CONCEPTS

In order to assess buckling safety, temperature-deflection and temperature-buckling energy relationships from the TSC dynamic buckling model are required. Buckling can be "explosive" (snap-through) or "progressive" (gradual displacements). For explosive buckling, distinct upper and lower buckling temperatures are identified (see points $T_{B,max}$ and $T_{B,min}$ in Figure 1). For progressive buckling, these two points coalesce at an inflection point (a "knee" on the curve). This knee can be construed to be a progressive buckling temperature (T_p), because beyond this value larger displacements occur.

Margin of Safety Definition and Buckling Response Classification

As discussed previously, buckling can occur at any temperature between $T_{B,max}$ and $T_{B,min}$, depending on the energy imparted to the track by the moving train. Defining $\Delta = T_{B,max} - T_{B,min}$, it can be shown that the buckling energy increases as Δ increases; hence, Δ can be construed as a margin of safety against buckling. Using this definition, the buckling response characteristics can be classified into three cases as shown in Figure 10:

- Case I represents tracks exhibiting a buckling response for which $\Delta > 20°F$,
- Case II represents tracks exhibiting a buckling response for which $20°F > \Delta > 0$, and
- Case III represents tracks exhibiting a progressive buckling response, $\Delta = 0$.

Figure 11 shows specific examples of these respective characteristics, including the energy required for buckling at $T_{B,min}$ (E_{max}) and the temperature above $T_{B,min}$ corresponding to the 50 percent E_{max}. For the example shown, it takes four times the energy to buckle at $T_{B,min}$ for Case I than for Case II. This becomes important in defining required levels of safety based on low versus moderate risks of buckling potential.

Levels of Safety

Based on previous discussions of buckling strength characteristics, analytic considerations, dynamic buckling tests, and railroad industry response, Figure 12 summarizes buckling safety concepts based on two levels of safety. These levels of safety have been devised to provide a minimum (low) risk

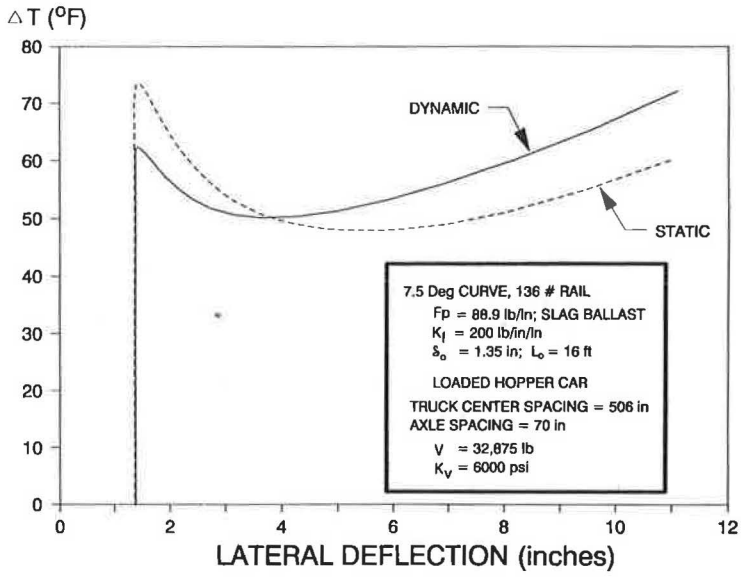

FIGURE 7 Influence of vehicle load on buckling response.

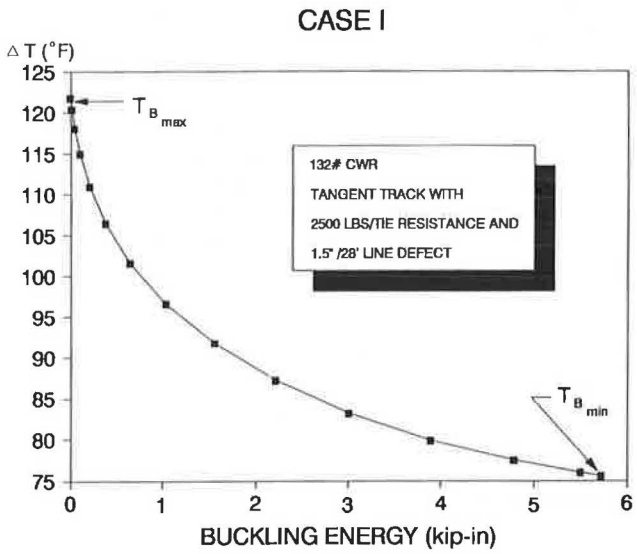

FIGURE 8 Buckling energy variation with temperature (tangent track).

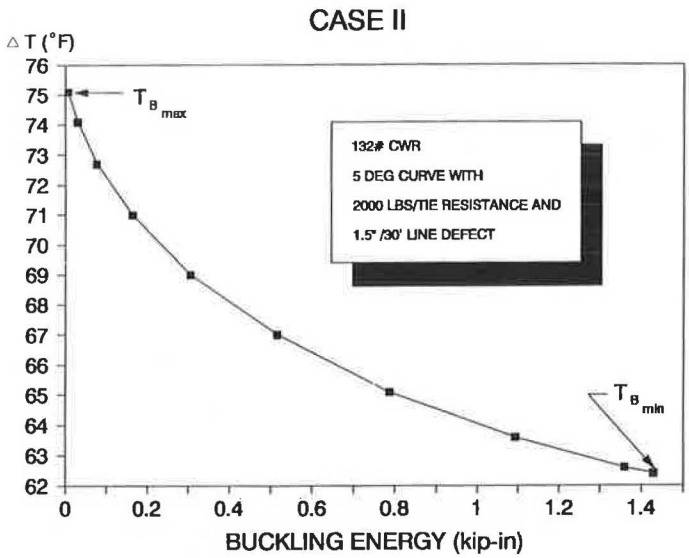

FIGURE 9 Buckling energy variation with temperature (curved track).

buckling potential and a marginal (moderate) risk buckling potential as illustrated in Figure 13:

- Level 1 safety (low-risk buckling potential) is based on $T_{B,\min}$, $T_{B,\min}$-20°F and T_p-20°F for Cases I, II, and III, respectively, for allowable temperature increase T_{ALL}, above neutral. The $T_{B,\min}$ limit for Case I is justified by the typically high buckling energies at this temperature and by the fact that the actual $T_{B,\min}$ values for Case I tracks tend to be higher than attained in most operating environments in the United States. The $T_{B,\max}$-20°F limit is based on the moderately low buckling energies associated with Case II type tracks. The rationale for the 20°F safety margin is the need to account for some of the dynamic effects not included in the analysis. These include braking and traction forces, truck hunting forces, impact loads, and vibration-induced loss of track resistance. This 20°F safety margin also has some experimental basis, as shown in the next section. The T_p-20°F limit for tracks with progressive characteristics (Case III) is based on the relatively small lateral displacements associated with this temperature, a requirement to limit misalignment growth and lateral deflection to small values, and test results indicating that initiation of misalignment growth tends to occur approximately 20°F below the T_p value.

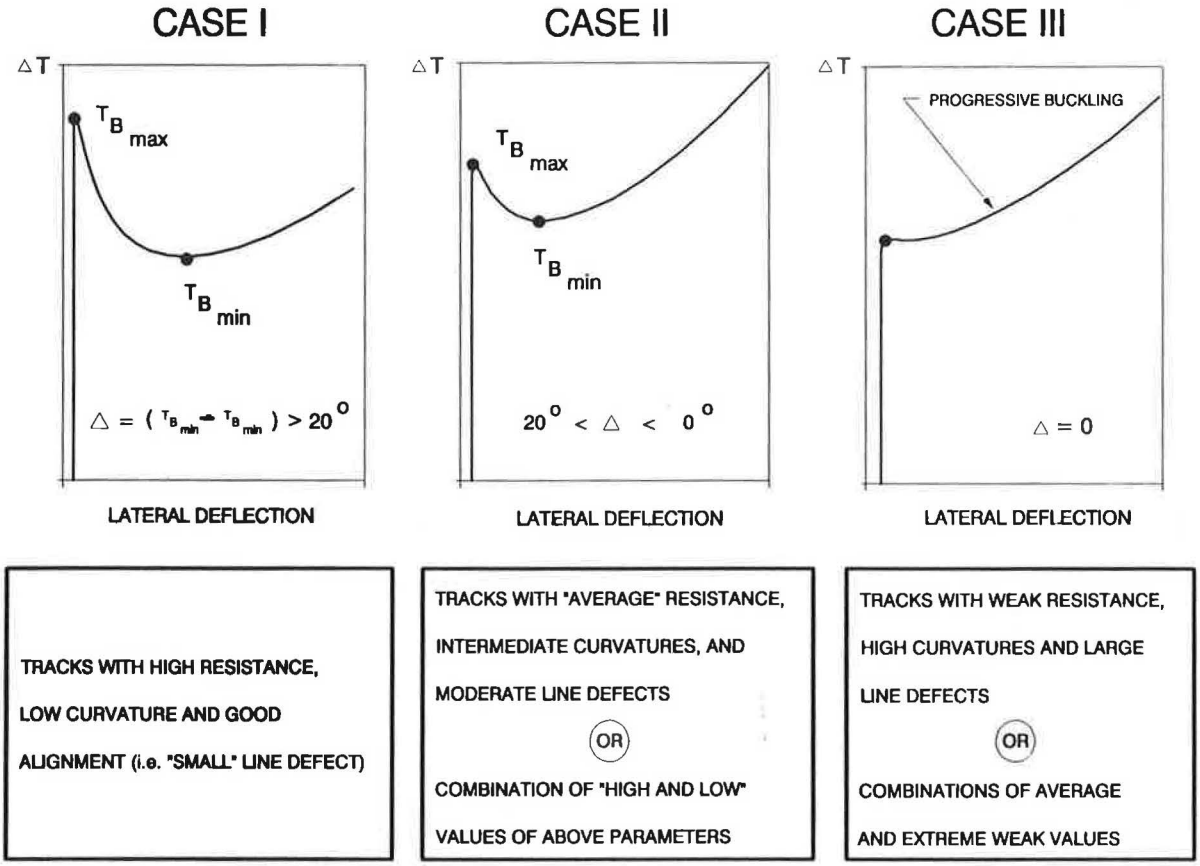

FIGURE 10 Classification of buckling characteristics.

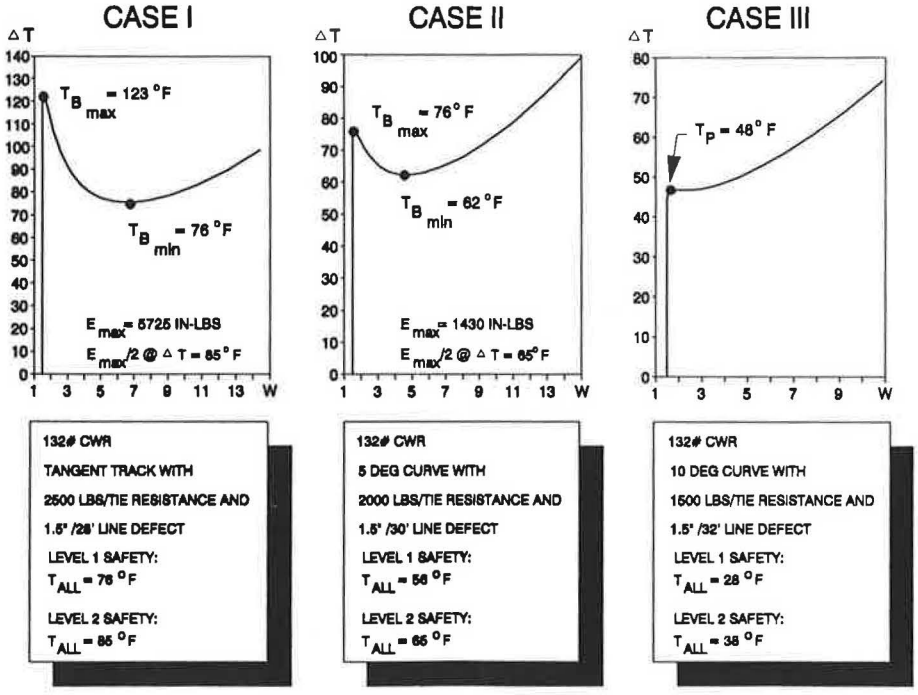

FIGURE 11 Typical buckling response examples.

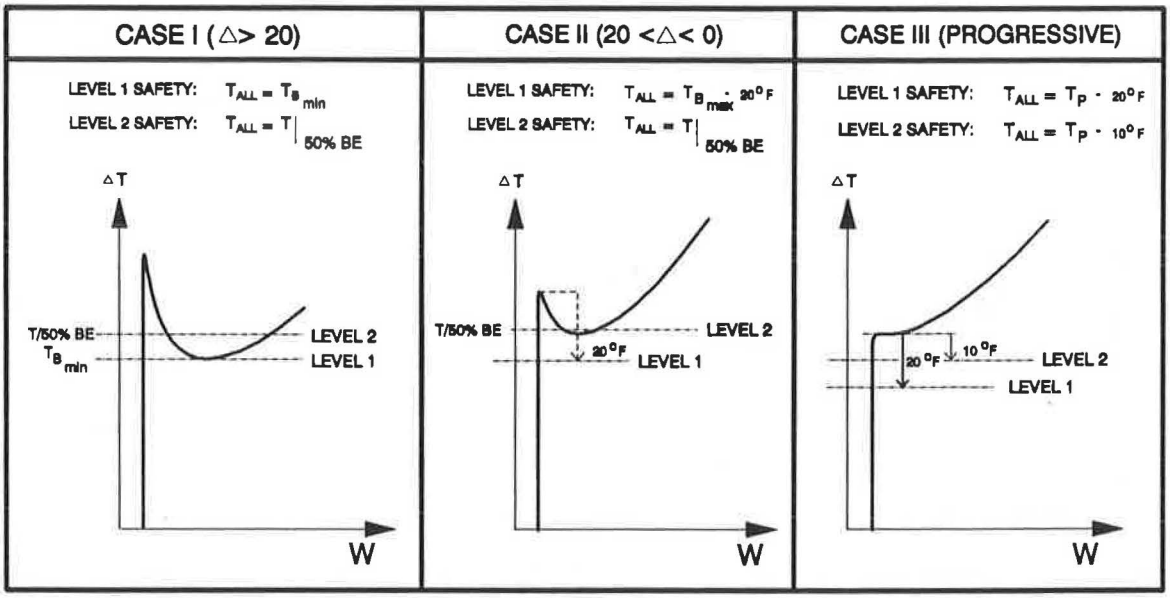

FIGURE 12 Safety criteria illustrations of levels of buckling safety.

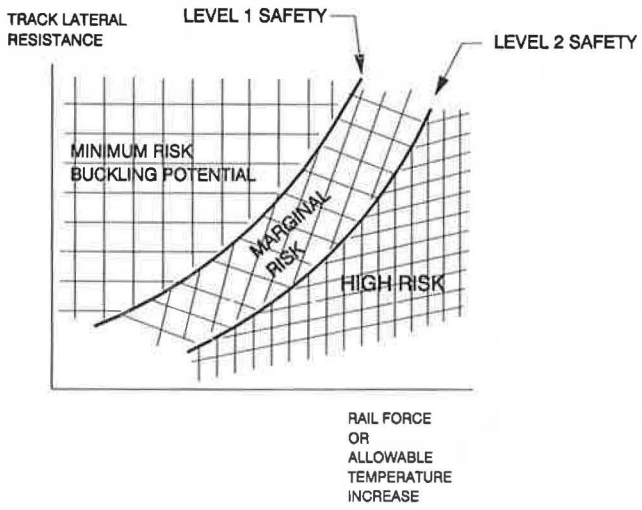

FIGURE 13 Illustration of prototype buckling safety criteria.

• Level 2 safety (moderate-risk buckling potential) is based on T (50 percent buckling energy) and T_p-10°F for allowable temperature increase values for Cases I, II, and III, respectively. The T limit is based on the supposition that Case I and II tracks can probably tolerate temperature increases above the $T_{B,min}$ value, as seen in some tests presented in the next section. The temperature corresponding to the 50 percent buckling energy value (recall that at $T_{B,min}$ the buckling energy is 100 percent) is an interim recommendation pending further research. The T_p-10°F value for Case III tracks is based partly on test results for progressive buckling response, and on industry consensus that even at the T_p value, Case III tracks (typically with high degrees of curvatures and low operating speeds) can probably tolerate train traffic at an acceptable level of risk.

The Level 2 safety limit values proposed are recommended only for those railroad institutions willing to maintain tracks to closer tolerances and implement CWR installation practices that adequately control the rail neutral temperature and hence the maximum force levels. Figure 11 provides specific examples of Levels 1 and 2 safety limits for Cases I, II, and III category tracks. Figure 13 illustrates sample prototype safety criteria in terms of allowable temperature increase (or rail force) for various levels of track resistance.

DYNAMIC BUCKLING TESTS

Dynamic buckling tests were carried out during 1983–1984 and 1986–1987 in the United States at the Transportation Test Center, in Pueblo, Colorado, on tangent and curved CWR tracks. Detailed summaries of these tests are given elsewhere (*12–14*).

The principal objectives of these tests were

• Experimental validation of dynamic buckling theory and identification of significant parameters that influence CWR track buckling response under thermal and vehicle-induced loads.

• Determination of required margin of safety for verification of proposed safety concepts and limits.

Test Methodology

The test methodology consisted of heating the rail by electric current using substations or diesel locomotives. The test track

lengths varied but were of the order of 1,000 ft to minimize end effects and obtain uniform rail force distribution in the central segment of the test zone. Lateral misalignments were set intentionally in the test track, and all other existing misalignments were mapped using a track geometry car or stringlining techniques. The tracks were destressed and instrumented with longitudinal rail force and vehicle wheel load gages as well as displacement transducers to measure longitudinal, lateral, and vertical movements of the rails. Thermocouples were used to measure rail temperature. Data loggers and strip chart recorders were employed to record data at frequent intervals. Track resistance was measured by both panel pull tests and STPTs. The number of cars in the test consist varied up to 70, depending on the tests.

Dynamic Buckling Theory Verification Tests

Comparison of Buckling Strength Under Hopper and Locomotive

To compare the relative influence of the central bending wave under a loaded 100-ton hopper and locomotive, equal levels of misalignment were set under each of the vehicles. Vertical and lateral displacements were measured as the rails were heated. Figure 14 shows a comparison of lateral displacements under each vehicle as a function of temperature. The misalignment growth under the hopper car is much more severe, indicating the influence of the longer uplift wave present under the 100-ton hopper car. The uplift wave is a contributing factor in the misalignment growth mechanism and hence a critical component of the dynamic buckling analysis. Subsequent dynamic tests and Figure 15 further confirm this uplift wave influence.

In another test, the measured response of the track with a large misalignment under a stationary hopper car favorably compared with the theoretical prediction (Figure 16). This test facilitated determination of lower buckling temperature and progressive buckling characteristics.

Comparison of Static and Dynamic Strengths of CWR

A weak 5-degree curved track was tested dynamically by a locomotive and hopper car at slow speeds. After an increase in temperature of up to 40°F above neutral and five train passes, initial misalignment did not increase. Train passes made at temperatures above 40°F increased the misalignment; at 62°F, the curve buckled to a deflection of 9 in., as shown in Figure 15. The buckling response was in agreement with the dynamic theory, but more important, these tests gave the first indication of a 10 to 20°F dynamic factor of safety requirement (i.e., at the buckling temperature of 62°F minus 10 to 20°F, track deflections were still very small).

Effect of Uplift Wave and L/V

In several tests the growth of imperfections under the passage of different cars was monitored using strip chart recorders. Figure 17 shows a typical result from the charts. The significant influence of the central bending wave of the hopper car can be seen. In contrast, the locomotive did not increase the deflection, which is in agreement with the theoretical predictions.

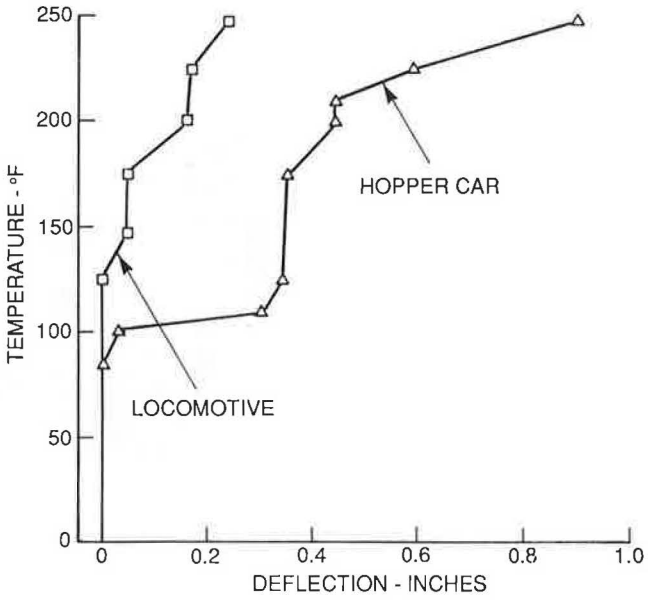

FIGURE 14 Response of track under vehicles.

Safety Concept Validation

Safety concepts and limits were partially verified on tangent, 5-, and 7.5-degree curved track as follows:

Tangent Track Tests (Tangents I and II)

In Tangent I with a lateral resistance (peak) value of 69.1 lb/in. and in Tangent II with a peak value of 89 lb/in., train passes were made at incremental heating levels. Results are shown in Table 1. The conditions represent Case I type tracks as referred to previously. No significant movement occurred at Level 1 safety limits. At higher temperatures attained in the test, the increase in misalignment was small; however, the vehicles were not operated at maximum allowable speeds.

5-Degree Curve Tests (Curves I and II)

Results for Curves I and II representing different peak resistance values are shown in Table 1. Again, the results are satisfactory from the Level 1 safety viewpoint. This is seen from the maximum temperatures reached in the test, which were in excess of the Level 1 temperatures.

7.5-Degree Curve

The objective in this test was not only to validate the Level 1 safety limit, but also to determine the ultimate buckling strength under a moving consist. The Level 1 safety limit of

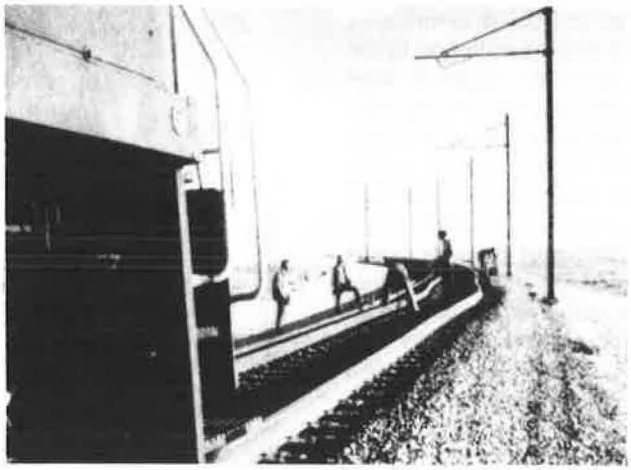

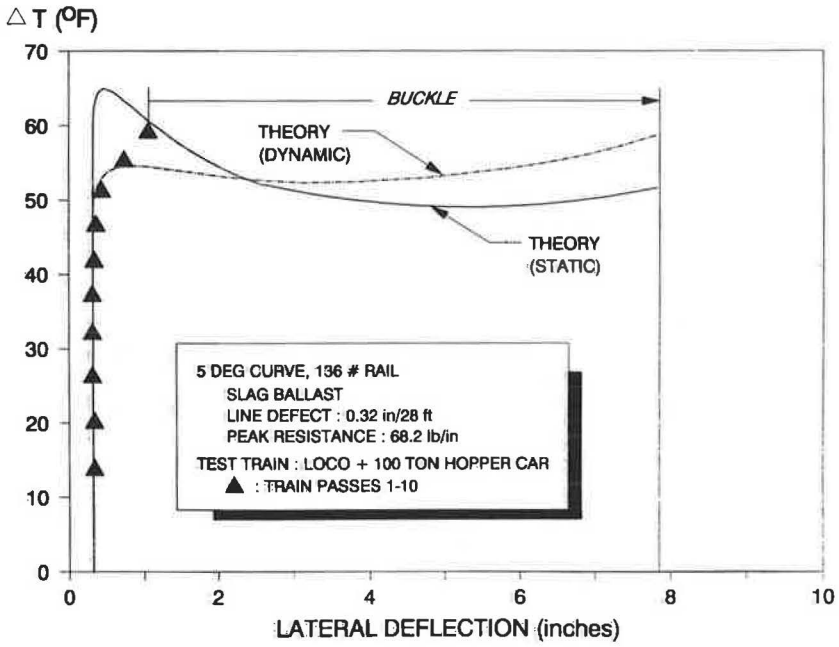

FIGURE 15 Dynamic buckling of curved track.

52°F was reached without causing significant increased misalignment due to vehicle passage. Analytical and experimental results are shown in Figure 18. At 62°F above the stress-free temperature, cumulative increased misalignment was experienced under the passage of each car. This misalignment resulted in a total deflection of 4.5 in. under the 12th car in the final run of the 24-car consist, before derailment at another location in the test zone stopped the test. Figures 19 and 20 present a view of the track and a derailed car. The test shows that the track can withstand Level 1 safety limit temperatures, and that buckling occurred below $T_{B,\max}$ and above $T_{B,\min}$.

CONCLUSIONS

- A versatile buckling model that can be run on a PC has been developed. The new model overcomes the deficiencies in other models, namely, absence of vehicle load effects, inadequate idealization of nonlinear lateral resistance, and lack of rational safety criteria. The model accounts for the loss of lateral resistance caused by a track uplift bending wave under vehicle loads. It also considers the softening behavior of the lateral resistance at large displacements, a phenomenon that has not been recognized in previous work. The model computes the energy required to precipitate buckling and thus

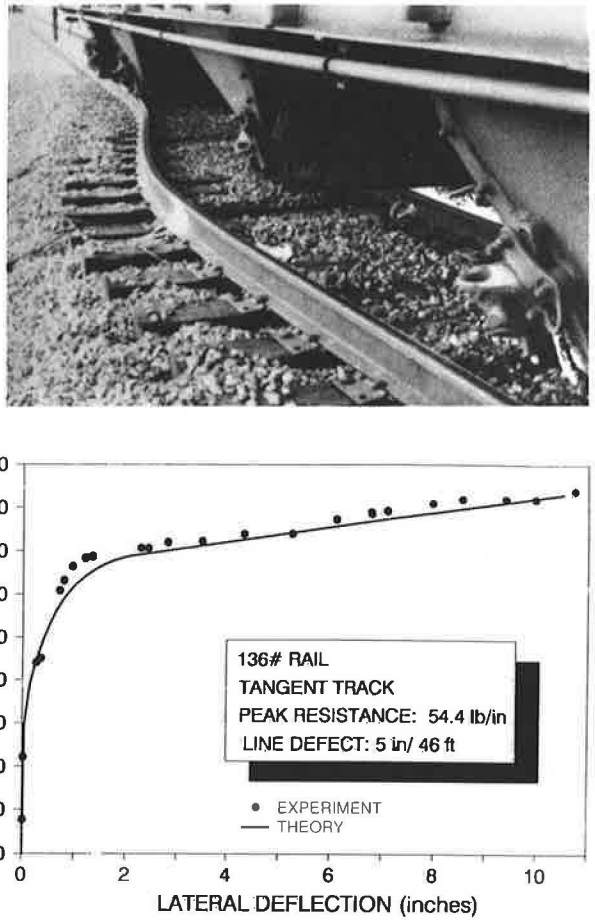

FIGURE 16 Dynamic buckling test (tangent).

evaluates the degree of safety of CWR at a given rail temperature.

- The model has been validated through several controlled, full-scale, dynamic buckling tests in which rails were artificially heated, and a long consist of cars made several passes at full speed over tracks with initial misalignments. Tangent, 5-, and 7.5-degree curves were tested in the validation of the dynamic model. Static tests, which showed higher buckling strengths in the absence of train traffic, were also performed.
- Vehicle vertical loads create precession or recession and central uplift bending waves in the track. For cars with large truck center spacing (hopper) the central uplift wave is critical, whereas for smaller truck center spacing cars (locomotive) the precession wave has more significant influence on buckling.
- In general, the growth of lateral misalignment under a vehicle is caused by a central bending wave rather than L/V. The influence of L/V can be significant for high impact loads and weak resistance tracks.
- The softening behavior of the lateral resistance is important in the analysis because it will have a significant influence on the lower buckling temperature. Idealizing the resistance as a constant at the peak value overestimates this temperature.
- The upper buckling temperature is sensitive to the peak value of the lateral resistance, the track misalignments, and the car parameters.
- Buckling safety limits are best approached on the basis of the energy levels required to buckle the track. Level 1 and 2 safety limits are introduced in this paper for low and moderate risks associated with track safety. The Level 1 limit has a margin of safety of at least 20°F, whereas Level 2 has a lower margin of safety. Level 1 safety limits have been verified for the tangent, 5-, and 7.5-degree curves through full-scale tests.

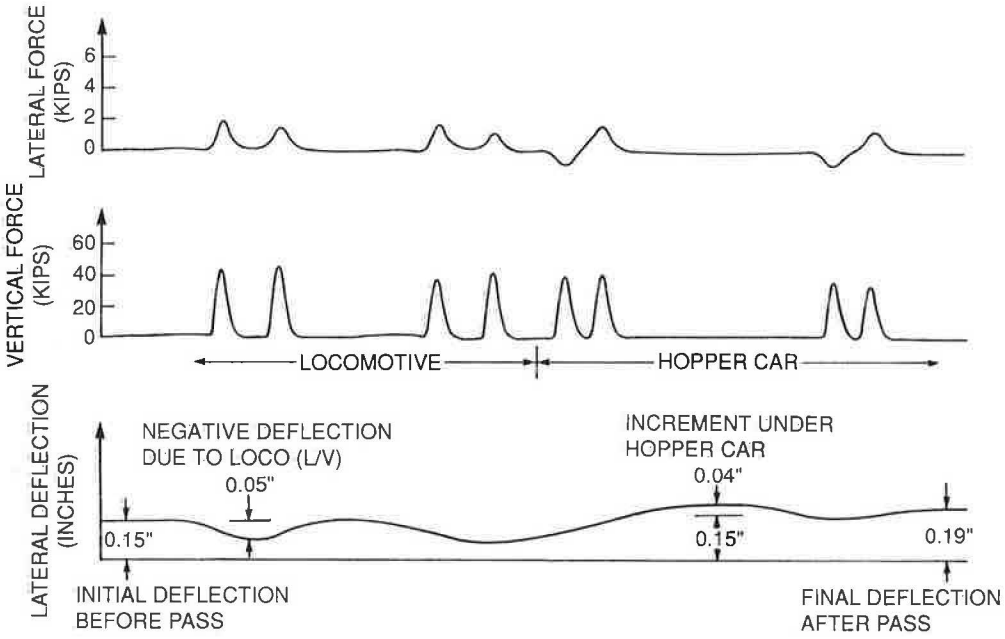

FIGURE 17 Strip chart record for pass no. 8 (curve with finite margin of safety).

TABLE 1 SUMMARY OF SAFETY LIMIT TESTS

TANGENT I	*PASS #*	*1*	*2*	*3*	*4*	*5*	*6*	*7*	*8*
N = 48	**ΔT (°F)**	61	71	81	80	88	86	93	92
V = 20	**P (kips)**	157	182	208	207	228	222	239	237
	δ_0 (in.)	0.88	0.89	0.91	0.91	0.94	0.95	0.98	0.99

TANGENT II	*PASS #*	*1*	*2*	*3*	*4*	*5*	*6*	*7*	*8*
N = 67	**ΔT (°F)**	70	76	83	82	85	95	100	100
V = 55	**P (kips)**	181	196	213	211	221	246	259	259
	δ_0 (in.)	0.81	0.83	0.86	0.87	0.78	0.79	0.81	0.82

CURVE I	*PASS #*	*1*	*3*	*5*	*7*	*9*	*11*	*13*	*15*	*16*	*17*
N = 63	**ΔT (°F)**	10	18.5	31	40	50	61	61	68	69	70
V = 20	**P (kips)**	25	48	81	104	129	158	157	175	179	180
	δ_0 (in.)	0.55	0.48	0.47	0.48	0.48	0.53	0.49	0.54	0.52	0.54

CURVE II	*PASS #*	*1*	*2*	*3*	*4*	*5*	*6*	*7*
N = 52	**ΔT (°F)**	39	64	68	56	66	72	80
V = 20	**P (kips)**	101	165	176	148	170	186	205
	δ_0 (in.)	0.50	0.55	0.58	0.70	0.75	0.79	0.84

TEST TRACK	*Fp (lb/in)*	*LEVEL 1 SAFETY LIMIT*	*ΔT_{test}*
TANGENT I	69.1	63	93
TANGENT II	80.0	65	100
CURVE I	83.7	59	70
CURVE II	100.0	60	80

N = Number of cars; V = Speed in mph; δ_0 = Line defect amplitude; P = Rail force

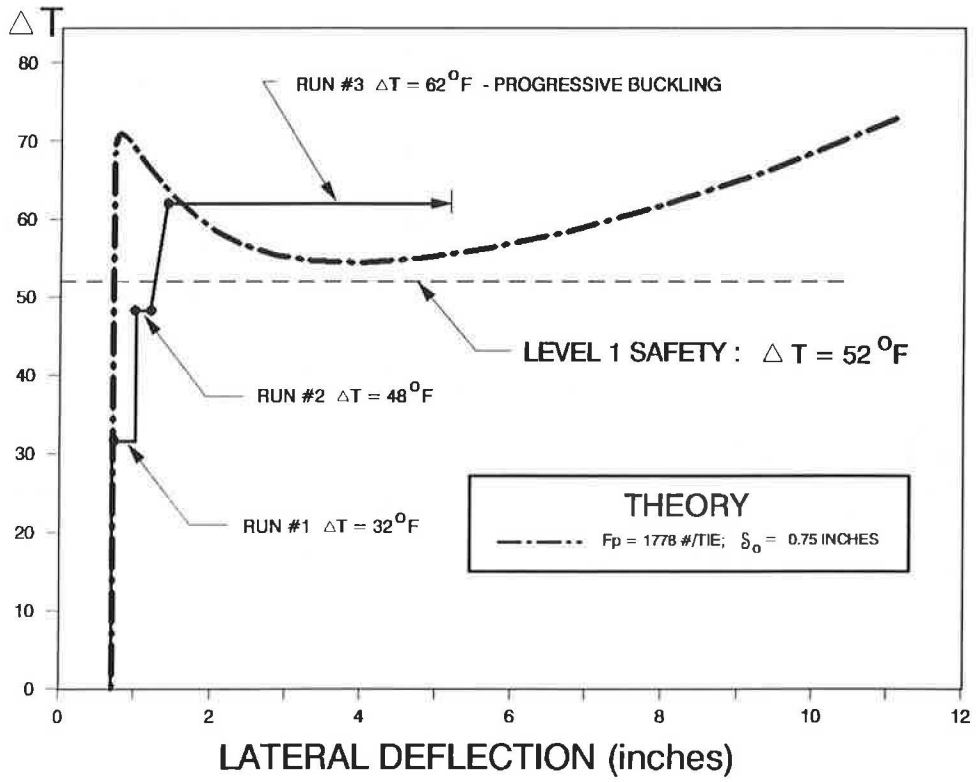

FIGURE 18 Dynamic buckling test analysis versus experiment.

FIGURE 19 Track condition after derailment.

FIGURE 20 Last car derailed.

ACKNOWLEDGMENTS

The authors wish to thank D. Jeong and M. Thurston for the development of the dynamic buckling software on the PC.

REFERENCES

1. A. D. Kerr. *Analysis of Thermal Track Buckling in the Lateral Plane.* Report DOT/FRA/ORD-76/285. FRA, U.S. Department of Transportation, 1976.
2. G. Samavedam. *Buckling and Post Buckling Analyses of CWR in the Lateral Plane.* Technical Note TN-TS-34. British Railways Board, London, 1979.
3. A. Kish, G. Samavedam, and D. Jeong. *Analyses of Thermal Buckling Tests on U.S. Railroads.* Report DOT/FRA/ORD-82/45. FRA, U.S. Department of Transportation, 1982.
4. G. Samavedam, A. Kish, and D. Jeong. *Parametric Studies on Lateral Stability of Welded Rail Track.* Report DOT/FRA/ORD-83/07. FRA, U.S. Department of Transportation, 1983.
5. A. Kish, G. Samavedam, and D. Jeong. *Influence of Vehicle Induced Loads on the Lateral Stability of CWR Track.* Report FRA/ORD-85-3. FRA, U.S. Department of Transportation, 1985.
6. F. Amans and R. Sauvage. Railway Track Stability in Relation to Transverse Stresses Exerted by Rolling Stock: A Theoretical Study of Track Behavior (in French), *Annales des Ponts et Chaussées*, No. 1, Jan.–Feb. 1969.
7. A. M. Zarembski and G. Magee. *An Investigation of Railroad Maintenance Practices to Prevent Track Buckling.* AAR Report R-454. Association of American Railroads, Washington, D.C., 1980.
8. J. Nagy. Experimental Investigations on CWR Track Behavior Due to Thermally Induced Loads, V (in Hungarian), In *Yearbook of the Hungarian Railway Scientific Research Institute*, 1970.
9. J. Nagy. Experimental Investigations on CWR Track Behavior Due to Thermally Induced Loads, VI (in Hungarian), In *Yearbook of the Hungarian Railway Scientific Research Institute*, 1974.
10. J. Eisenmann. The Significance of the Rail Lifting Wave. *Rail International*, No. 10, Oct. 1976, pp. 576–581.
11. G. Samavedam, A. Kish, M. Thurston, and D. Jeong. Recent Advances in Track Buckling Mechanics. Applied Mechanics Rail Transportation Symposium, AMD, Vol. 96, RTD, Vol. 2, 1988.
12. G. Samavedam, A. Kish, and D. Jeong. *Experimental Investigations of Dynamic Buckling of CWR Tracks.* Report DOT/FRA/ORD-86/07. FRA, U.S. Department of Transportation, 1986.
13. A. Kish and G. Samavedam. *Analyses of Phase III Dynamic Buckling Tests.* Final Report DOT/FRA/ORD-89/08. FRA, U.S. Department of Transportation, 1989.
14. G. Samavedam and A. Kish. *Dynamic Buckling Test Analyses of a High Degree CWR Track.* Report DOT/FRA/ORD-85/03. FRA, U.S. Department of Transportation, 1989.